



Supplement of

Amplified role of potential HONO sources in O₃ formation in North China Plain during autumn haze aggravating processes

Jingwei Zhang et al.

Correspondence to: Weigang Wang (wangwg@iccas.ac.cn) and Junling An (anj@mail.iap.ac.cn)

The copyright of individual parts of the supplement might differ from the article licence.

Sect. S1. Definitions of MB, NMB, RMSE and IOA

The statistical measures used in this study are mean bias (MB), normalized mean bias (NMB), root mean squared error (RMSE) and index of agreement (IOA). The MB, NMB, RMSE and IOA are calculated as:

$$MB = \frac{\sum_{i=1}^N (P_i - O_i)}{N}$$

$$NMB = \frac{\sum_{i=1}^N (P_i - O_i)}{\sum_{i=1}^N O_i} \times 100\%$$

$$RMSE = \sqrt{\frac{\sum_{i=1}^N (P_i - O_i)^2}{(N-1)}}$$

$$IOA = 1 - \frac{\sum_{i=1}^N (O_i - P_i)^2}{\sum_{i=1}^N (|P_i - \bar{O}| + |O_i - \bar{O}|)^2}$$

Where P_i represents the simulated data and O_i represents the observed data. N means the number of data pairs. \bar{O} is the mean of observations.

Sect. S2. The enhanced DMA8 O₃ due to Het_{ground} with three f values (cases F_half, F, and F_double) is shown in **Fig. S13**, the enhancements in hazy days were about two times those in clean days. Choosing the three f values ($f = 0.04 \times (1 + SR/100)$, $0.08 \times (1 + SR/100)$, and $0.10 \times (1 + SR/100)$, respectively) enhanced ~ 1 ppb, ~ 1.5 ppb and ~ 2 ppb of DMA8 O₃ in clean days, respectively; and ~ 2 – 2.5 ppb, ~ 3 – 4 ppb and ~ 4 – 5 ppb of DMA8 O₃ in hazy days, respectively. The DMA8 O₃ enhancement in the haze aggravating process was slightly increased by ~ 0.5 ppb for the smaller f of $0.04 \times (1 + SR/100)$, and was increased by ~ 1 ppb for the larger f of $0.10 \times (1 + SR/100)$.

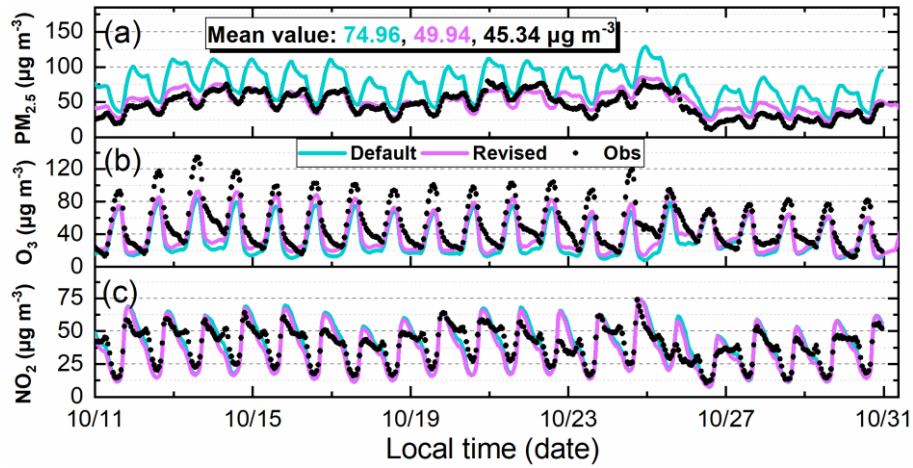


Fig. S1 Comparison of 95-site-averaged simulations (default and revised emissions for the base case) and observations of hourly $\text{PM}_{2.5}$, O_3 and NO_2 in the North China Plain during Oct. 11–30 of 2018.

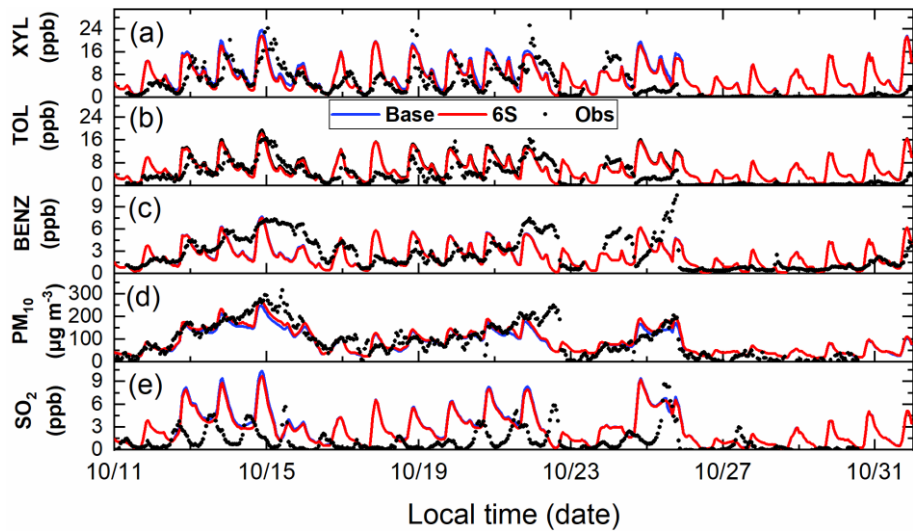


Fig. S2 Comparison of simulated (Base and 6S cases) and observed hourly concentrations of xylenes (XYL), toluene (TOL), benzene (BENZ), PM_{10} and SO_2 at the BUCT site during Oct. 11–31 of 2018.

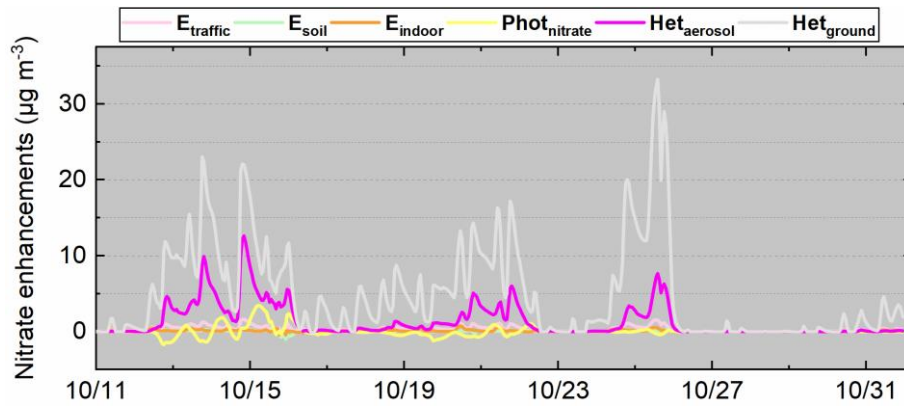


Fig S3 Nitrate enhancements due to each of the six potential HONO sources at the BUCT site during Oct.11–31 of 2018.

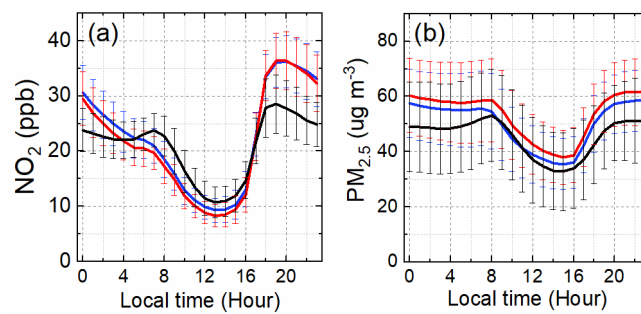


Fig S4 Diurnal comparison of 95-site-averaged simulated (Base and 6S cases) and observed NO_2 (a) and $\text{PM}_{2.5}$ (b) in the North China Plain during Oct.11–31 of 2018.

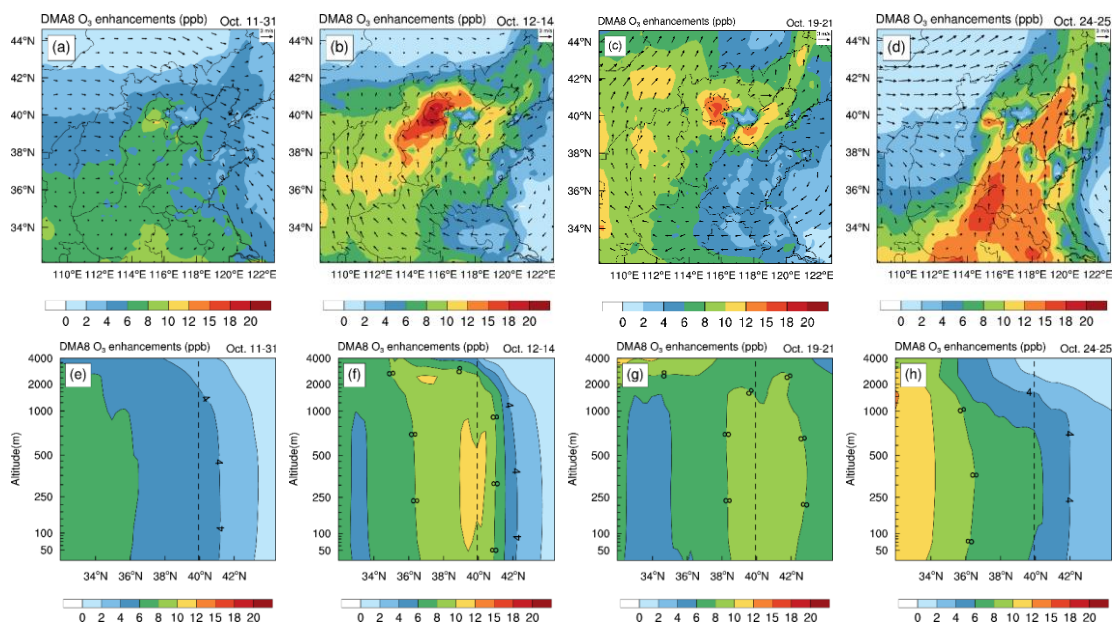


Fig.S5 Surface-averaged (a–d) and zonal-averaged (e–h) DMA8 O_3 enhancements due to the six potential HONO sources in the North China Plain during the study period (Oct.11–31, 2018) and the three haze aggravating periods (Oct.12–14, Oct. 19–21 and Oct.24–25) (The dashed line denotes the latitude of the BUCT site).

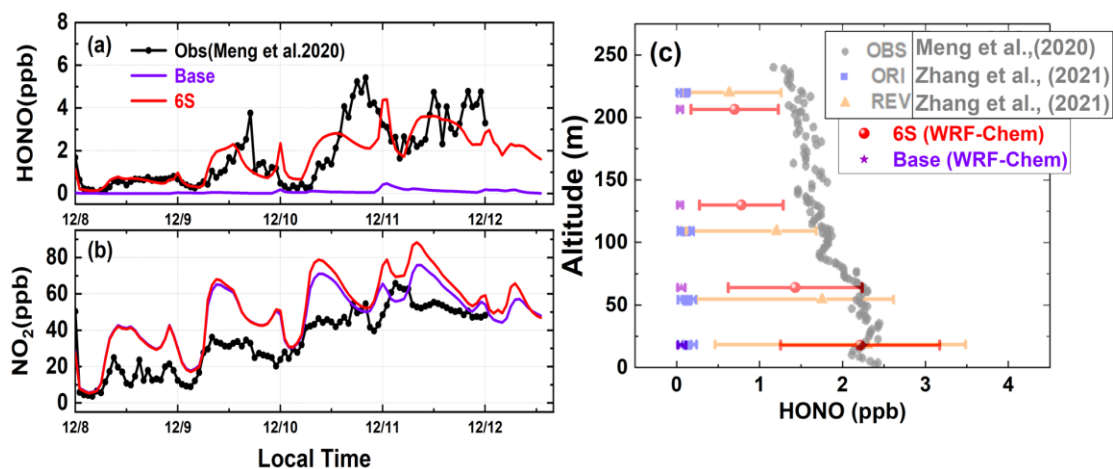


Fig.S6 Comparison of simulated (Base and 6S cases) and observed hourly concentrations of HONO (a) and NO_2 (b) at the IAP site during Dec.08–12 of 2016, and comparison of simulated (Base and 6S were in this study, ORI and REV were from Zhang et al. (2021)) and observed vertical HONO profiles during nighttime (19:00–05:59) of Dec.09-12, 2016 (The observations were obtained from Meng et al. (2020), the right panel were modified from **Fig.1c** in Zhang et al. (2021) for comparison).

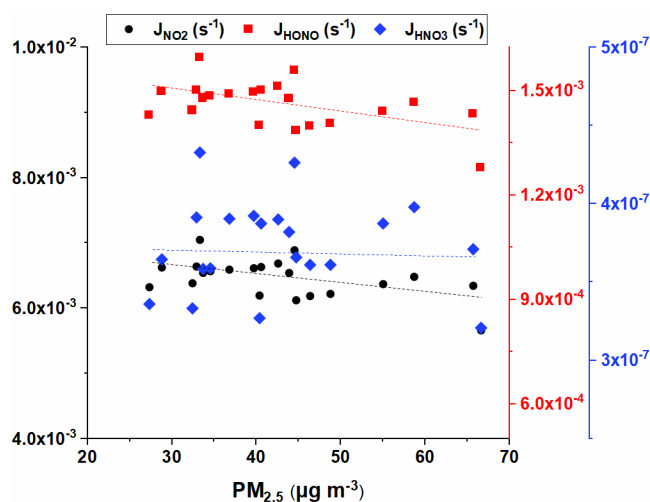


Fig.S7 The 95-NCP-site-averaged relationship between surface $\text{PM}_{2.5}$ and photolysis frequencies of NO_2 , HONO and HNO_3 for the 6S cases during Oct.11–31, 2018.

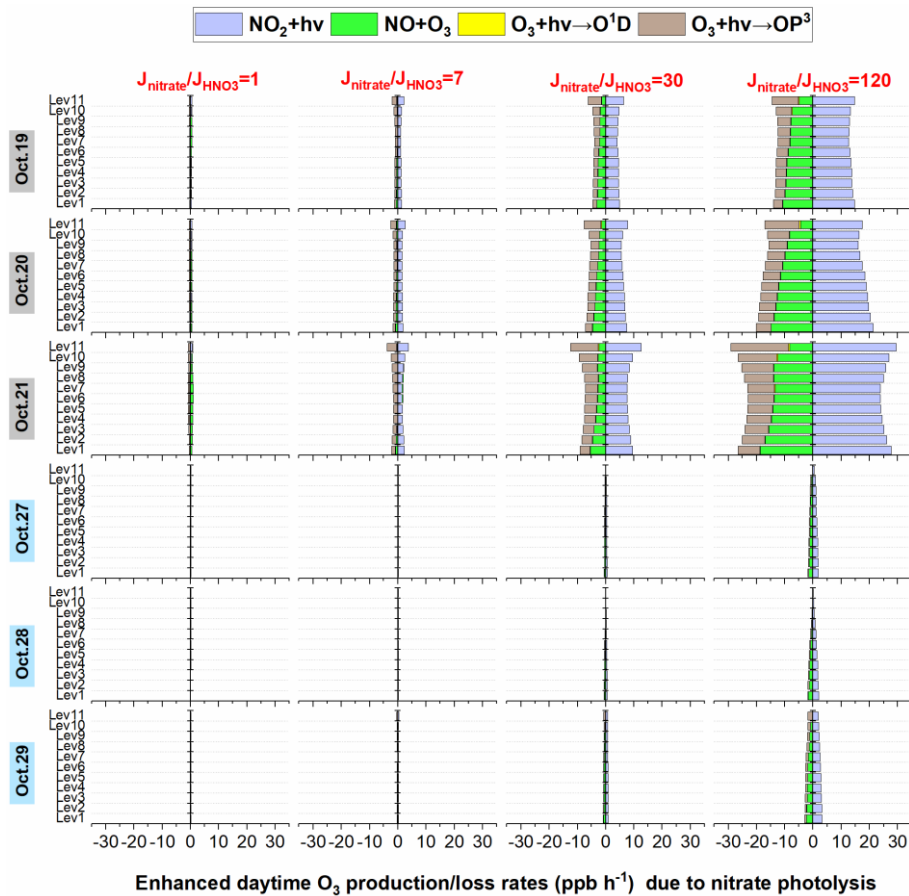


Fig S8 Daytime-averaged enhancements of major O_3 production/loss rates caused by $Phot_{nitrate}$ with four $J_{nitrate}/J_{HNO_3}$ ratios (1, 7, 30 and 120) during a typical haze aggravating process (Oct.19–21) and clean days (Oct.27–29).

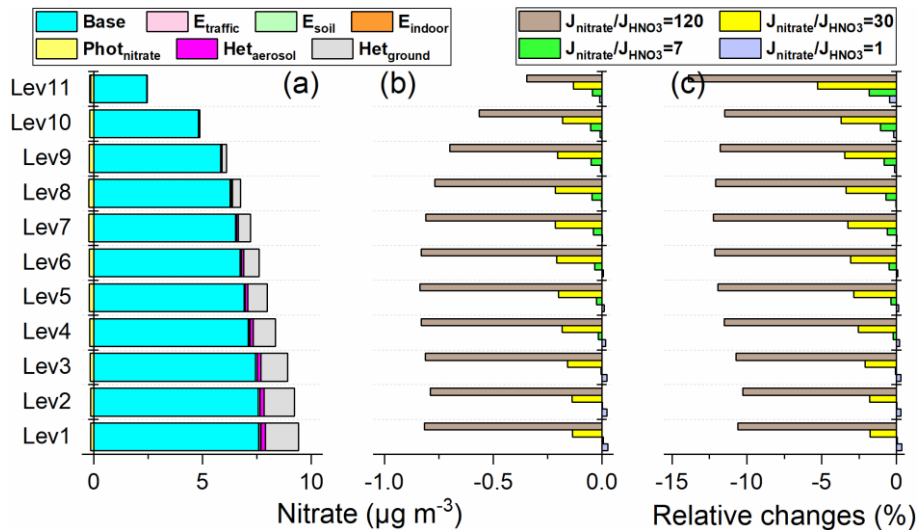


Fig.S9 The 95-NCP-site-averaged nitrate concentration for the base case and the nitrate enhancements induced by the six potential HONO sources (a), the nitrate variations with four $J_{nitrate}/J_{HNO_3}$ ratios (1, 7, 30 and 120) (b) and corresponding relative changes compared with the

base case (c) during Oct.11–31 of 2018.

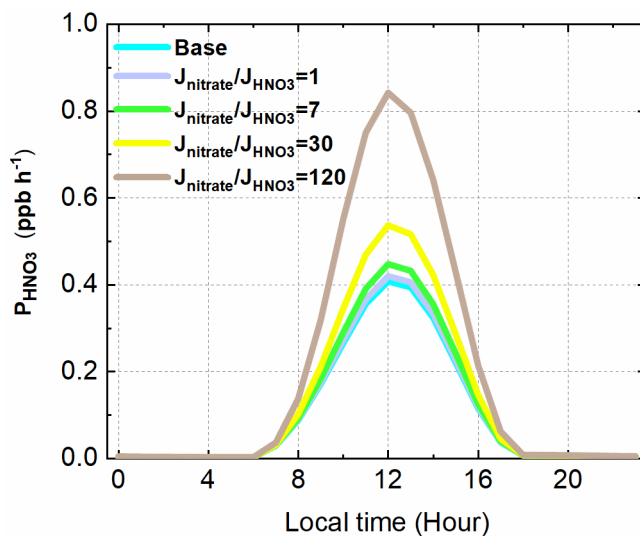


Fig.S10 Comparison of vertical-averaged HNO₃ production rates at 95 NCP sites for the base case and four cases with different $J_{\text{nitrate}}/J_{\text{HNO}_3}$ ratios (1,7,30 and 120) during the study period.

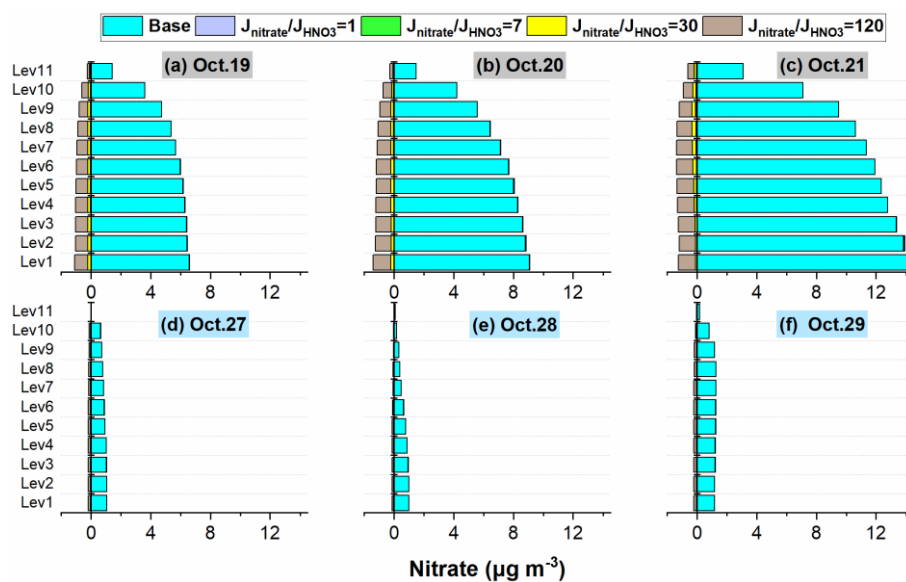


Fig.S11 The 95-NCP-site-averaged changes of nitrate with four $J_{\text{nitrate}}/J_{\text{HNO}_3}$ ratios (1, 7, 30 and 120) compared with the base case during a typical haze aggravating process of Oct.19–21 (a–c) and a clean period of Oct.27–29 (d–f) of 2018.

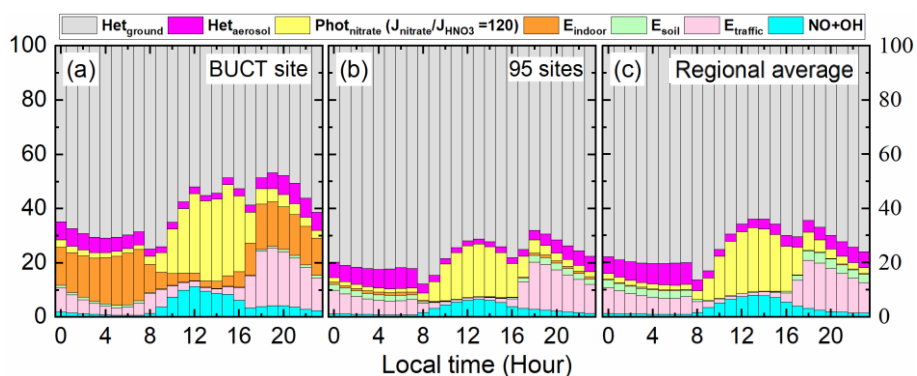


Fig.S12 The relative contributions of the six potential HONO sources and the reaction of OH with NO to surface HONO concentrations for the 6S case at the BUCT site (a), 95 monitoring sites (b) and in the whole region (c). Note the $J_{\text{nitrate}}/J_{\text{HNO}_3}$ ratio was 120 here, while the $J_{\text{nitrate}}/J_{\text{HNO}_3}$ was 30 in Fig.3.

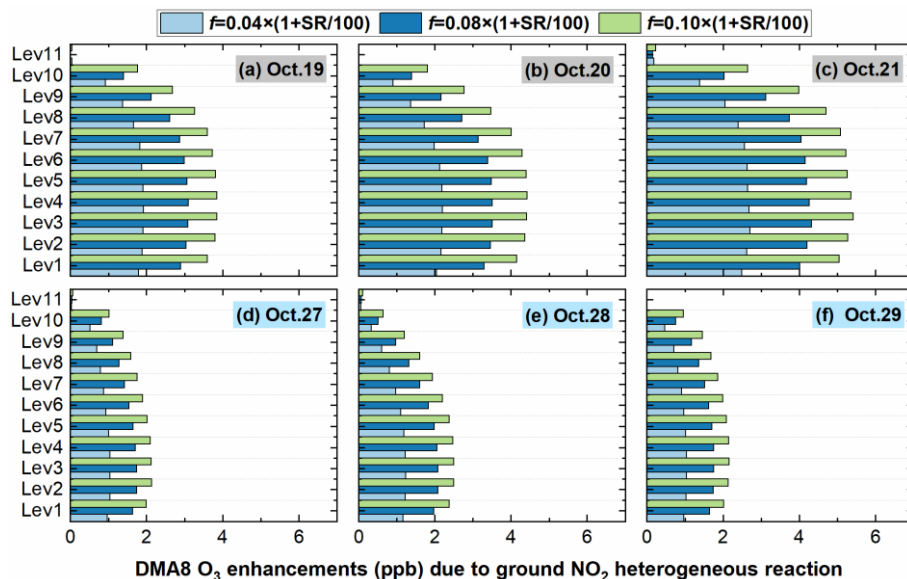


Fig.S13 The 95-NCP-site-averaged DMA8 O₃ enhancement induced by the NO₂ heterogeneous reaction with three f values during a typical haze aggravating process of Oct.19–21 (a–c) and a clean period of Oct.27–29 (d–f) of 2018.

- Meng, F., Qin, M., Tang, K., Duan, J., Fang, W., Liang, S., Ye, K., Xie, P., Sun, Y., Xie, C., Ye, C., Fu, P., Liu, J., and Liu, W.: High-resolution vertical distribution and sources of HONO and NO₂ in the nocturnal boundary layer in urban Beijing, China, *Atmos. Chem. Phys.*, 20, 5071–5092, <https://doi.org/10.5194/acp-20-5071-2020>, 2020
- Zhang, S., Sarwar, G., Xing, J., Chu, B., Xue, C., Sarav, A., Ding, D., Zheng, H., Mu, Y., Duan, F., Ma, T., and He, H.: Improving the representation of HONO chemistry in CMAQ and examining its impact on haze over China, *Atmos. Chem. Phys.*, 21, 15809–15826, <https://doi.org/10.5194/acp-21-15809-2021>, 2021.